eGastroenterology

Characterisation of HBV and co-infection with HDV and HIV through spatial transcriptomics

Amy Cross,[1] James M Harris ,[2] Edward Arbe-Barnes,[3] Colin Nixon,[4] Rageshri Dhairyawan,[5,6] Andrew Hall,[7] Alberto Quaglia,[7] Fadi Issa,[1] Patrick T F Kennedy,[6] Jane A McKeating,[2,8] Upkar S Gill,[6] Dimitra Peppa [3]

To cite: Cross A, Harris JM, Arbe-Barnes E, *et al*. Characterisation of HBV and co-infection with HDV and HIV through spatial transcriptomics. *eGastroenterology* 2024;**2**:e100067. doi:10.1136/egastro-2024-100067

► Prepublication history and additional supplemental material for this paper are available online. To view these files, please visit the journal online (https://doi.org/10.1136/egastro-2024-100067).

USG and DP contributed equally.

Received 21 February 2024
Accepted 19 June 2024

For numbered affiliations see end of article.

Correspondence to
Dr Dimitra Peppa; d.peppa@ucl.ac.uk and Dr Upkar S Gill; u.gill@qmul.ac.uk

ABSTRACT

Background and aims The intrahepatic processes associated with chronic hepatitis B (CHB), especially in the context of hepatitis delta virus (HDV) and HIV co-infection, require a better understanding. Spatial transcriptomics can provide new insights into the complex intrahepatic biological processes, guiding new personalised treatments. Our aim is to evaluate this method characterising the intrahepatic transcriptional landscape, cellular composition and biological pathways in liver biopsy samples from patients with hepatitis B virus (HBV) and HDV or HIV co-infection.

Method The NanoString GeoMx digital spatial profiling platform was employed to assess expression of HBV surface antigen and CD45 in formalin-fixed paraffin-embedded (FFPE) biopsies from three treatment-naïve patients with chronic HBV and HDV or HIV co-infection. The GeoMx Human Whole Transcriptome Atlas assay quantified the expression of genes enriched in specific regions of interest (ROIs). Cell type proportions within ROIs were deconvoluted using a training matrix from the human liver cell atlas. A weighted gene correlation network analysis evaluated transcriptomic signatures across sampled regions.

Results Spatially discrete transcriptomic signatures and distinct biological pathways were associated with HBV infection/disease status and immune responses. Shared features including 'cytotoxicity' and 'B cell receptor signalling' were consistent across patients, suggesting common elements alongside individual traits. HDV/HBV co-infection exhibited upregulated genes linked to apoptosis and immune cell recruitment, whereas HIV/HBV co-infection featured genes related to interferon response regulation. Varied cellular characteristics and immune cell populations, with an abundance of γδT cells in the HDV/HBV sample, were observed within analysed regions. Transcriptional differences in hepatocyte function suggest disrupted metabolic processes in HDV/HBV co-infection potentially impacting disease progression.

Conclusion This proof-of-principle study shows the value of this platform in investigating the complex immune landscape, highlighting relevant host pathways to disease pathogenesis.

WHAT IS ALREADY KNOWN ON THIS TOPIC

⇒ Limited studies visualising the liver microenvironment in chronic hepatitis B (CHB) and spatial distribution of immune infiltration and hepatitis B virus (HBV)-infected hepatocytes reveal heterogeneity.

⇒ This warrants further investigation to understand these relationships, specifically in the presence of co-infection.

WHAT THIS STUDY ADDS

⇒ The study demonstrated the utility of spatial transcriptomics to provide new insights into the complex interplay between host factors and viral infection in CHB and co-infection.

⇒ The high-resolution spatial maps generated through NanoString GeoMx digital spatial profiling technology allowed for in-depth analyses of gene expression patterns, immune cell compositions and biological processes within the liver microenvironment.

⇒ It highlighted the contribution of previously unappreciated immune cell subsets and identified shared and unique transcriptional signatures, emphasising the potential of spatial transcriptomics in understanding HBV pathogenesis impacted by co-infection.

HOW THIS STUDY MIGHT AFFECT RESEARCH, PRACTICE OR POLICY

⇒ The findings provide a foundation for future research aimed at improving the diagnosis and development of personalised treatments for HBV infection, especially in co-infection scenarios with hepatitis delta virus (HDV) and HIV.

INTRODUCTION

Chronic Hepatitis B (CHB) is a global health burden, presenting as a heterogenous disease with a high risk of hepatocellular carcinoma (HCC) and liver-related complications, causing over 800 000 deaths annually.[1] Hepatitis B (HBV) and delta (HDV) virus co-infection associates with severe viral hepatitis with an estimated 12 million cases worldwide.[2] HBV prevalence is disproportionately high among people with HIV,[3] with an increased risk of accelerated liver disease progression and increased mortality.[3–6] Current CHB treatments include nucleos(t)ide analogues that suppress virus replication but do not

target covalently closed circular DNA (cccDNA)[7] and rarely cure infection. Despite recent advances,[8] there is an urgent need for novel and/or personalised therapeutic approaches for the treatment of CHB.[9]

HBV infection has limited direct cytopathic effects and persistent expression of viral proteins such as HBV surface antigen (HBsAg) in the liver can perturb host innate and adaptive T cell responses.[10] HBsAg levels are associated with the severity of fibrosis and treatment responses,[11–13] with achieving sustained clearance of peripheral HBsAg and anti-HBs antibody seroconversion being critical goals of functional cure strategies.[14] Notably, CHB exhibits dynamic fluctuations in peripheral viral load and alanine aminotransferase (ALT) activity,[15] yet the relationship between these circulating markers, infected hepatocytes and localised inflammatory responses is unclear. Innate and adaptive cellular responses play a role in viral control and liver damage.[10 16] Balancing immune-mediated clearance without excessive hepatocyte killing is critical for HBV cure strategies, particularly in HDV/HBV and HIV/HBV co-infection, where intrahepatic responses remain underinvestigated.

Existing single-cell sequencing studies lack preserved liver tissue architecture,[17–19] limiting our understanding of spatial relationships in the liver. Imaging mass cytometry (IMC) and multiplex immunofluorescence have provided limited insights,[20] revealing heterogeneous patterns of viral antigen staining among patients with CHB. These studies identified distinct liver microenvironments/signatures that did not correlate with HBV antigen burden.[21 22]

Spatial transcriptomics, using the NanoString GeoMx digital spatial profiling (DSP) technology, offers a promising approach to visualise the topography of HBV-infected hepatocytes and to study gene expression patterns in distinct regions of interest (ROIs) within the CHB liver. This proof-of-principle study sets the groundwork for future comprehensive analyses, providing insights into the complex host-viral interplay in CHB and the potential influence of HDV and HIV co-infection.

METHODS

Patient samples and ethics

Archived formalin-fixed paraffin-embedded (FFPE) liver biopsies from three patients with chronic HBV (PT1), one with HDV/HBV co-infection (PT2) and one patient with HIV/HBV (PT3) co-infection were analysed in this study. Participants were recruited at The Royal London Hospital, Barts Health NHS Trust and samples were obtained during routine diagnostic procedures following written informed consent. Table 1 includes the demographic and clinical parameters of each participant. Each biopsy was evaluated by a histopathologist and scored for the degree of fibrosis (Ishak) and Hepatitis Activity Index.

NanoString GeoMx digital spatial profiling

Slides were submitted for DSP and whole transcriptome sequencing, according to the manufacturer's recommendations for GeoMx-NGS RNA BOND RX slide preparation (manual no. MAN-10131-02). The panel of morphology markers was designed to include HBsAg ((Polyclonal) 488 1:200 from Bioss #bs-1557G-A488), CD45 (D9M8I) 594 1:100 from Cell Signaling Technology #13917BF, CD3 (clone UMAB54; Origene #UM500048CF) and a DNA dye (Syto83dye; Invitrogen). Deparaffinisation, rehydration, heat-induced epitope retrieval (for 20 min at 100°C) and enzymatic digestion (1 µg/mL proteinase K for 15 min at

Table 1 Patient characteristics

	PT1: HBV	PT2: HDV/HBV	PT3: HIV/HBV
Sex	Male	Female	Male
Age range*	50s	40s	20s
Country of origin	China	Romania	India
ALT (IU/L)	30	48	160
HBsAg (IU/mL)	3405	20137	193874
HBeAg/HBeAb	Neg/Pos	Pos/Neg	Pos/Neg
HBV DNA (IU/mL)	190000	89247	235×10^6
HDV Ab	Neg	Pos	Neg
HDV RNA (cp/mL)	Neg	3600000	Neg
CD4	NA	NA	400
Ishak	0	5	1
HAI	2	6	9

All subjects were treatment naïve at liver biopsy sampling.
*Age at time of liver biopsy sampling.
Ab, antibody; ALT, alanine aminotransferase; HAI, Hepatitis Activity Index; HBeAb, hepatitis B e antibody; HBeAg, hepatitis B e antigen; HBsAg, HBV surface antigen; HBV, hepatitis B virus; HDV, hepatitis delta virus; NA, not available; Neg, negative; Pos, positive; PT1, patient 1; PT2, patient 2; PT3, patient 3.

37°C) were carried on the Leica BOND-RX. Tissues were incubated with 10% neutral buffered formalin for 5 min and for 5 min with NBF stop buffer. The tissue sections were hybridised with the oligonucleotide probe mix (Whole Transcriptome Atlas) overnight, then blocked and incubated with the four fluorescently labelled markers for 1 hour. Tissue sections were loaded into the GeoMx platform and scanned for an immunofluorescent signal. A geometric strategy was employed for selection of ROIs, which were segmented on the basis of HBsAg staining and CD45 staining to capture the presence of immune cell infiltrate (online supplemental figure 1A–C). ROI metadata are included in online supplemental table 1. The DSP barcodes were UV-cleaved and collected for each selected ROI and counted. During the library preparation, the DSP barcodes were tagged with their specific ROI location and RNA target identification sequence. Sequenced oligonucleotides were then processed and imported back into the GeoMx DSP platform for integration with the slide images and ROI selections for spatially resolved RNA expression. FASTQ sequencing files were processed into digital count conversion digital files using Nanostring GeoMx NGS Pipeline software.

Quality control and normalisation

Quality control checks and data analysis were performed in the GeoMx DSP Data Analysis suite. All ROIs had acceptable sequencing quality metrics after examination of the raw, trimmed, stitched, aligned and deduplicated reads, and the sequencing saturation (>60%; online supplemental figure 2B, C). An expression value per gene target per ROI was generated in GeoMx DSP Analysis Suite through the compilation of multiple probes, within the NanoString GeoMx Human Whole Transcriptome Atlas probe mix, for each transcript.

The manufacturer's recommended threshold for the detection of genes is referred to as the limit of quantification (LOQ); the LOQ is 2 geometric SD above the geometric mean. The ROIs from PT2, PT1 and PT3 tissues were filtered to include only the genes detected over the LOQ in 3 or more ROIs: 9672 genes. The data were then quantile normalised and the performance of the normalisation was assessed by the standardisation of housekeeping genes and distribution of total gene expression between ROI (online supplemental figure 2D, E).

Principal component analysis

The variance in the dataset was assessed by principal component analysis (PCA) of $\log_2(n+1)$ transformed of the quantile-normalised and gene-filtered expression values from the selected tissue samples and variance was associated with biological factors, such as tissue identity, estimated immune infiltrate and estimated HBsAg expression. The contributing genes to the PCA analysis are included in online supplemental table 2.

Over-representation analyses

Differential gene expression was calculated using linear mixed models with fixed effects of immune presence or HBsAg presence in R package Limma V.3.56.2. P values were unadjusted in the figures and both unadjusted and adjusted using the Benjamini-Hochberg method in online supplemental table 3. Over-representation analysis for Gene Ontology Biological Processes (GO.BP) terms was performed on genes showing >1.5-fold change and p value <0.05 using R package clusterProfiler (V.4.8.2). Analysis parameters included a p value cut-off of 0.05 and a q value cut-off of 0.1. Redundant and duplicated pathways were excluded from figures. For the complete list of pathways with both unadjusted and adjusted values, refer to online supplemental table 4.

Cell deconvolution

Cell deconvolution analyses were generated in the GeoMx DSP control centre, using the spatialdecon geoscript (V.1.1, updated April 2021) available at Nanostring's Geoscript Hub (https://nanostring.com/products/geomx-digital-spatial-profiler/geoscript-hub/). The analyses were run using the adult liver landscape 10x matrix (https://github.com/Nanostring-Biostats/CellProfileLibrary). Cell abundances were estimated using the SpatialDecon R library, which performs mixture deconvolution using constrained log-normal regression. The 0.75 quantile-scaled data were used as input.[23]

Weighted gene correlation network analysis

The weighted gene correlation network analysis (WGCNA) was applied to the quantile normalised and filtered expression values, which were then transformed by $\log_2(n+1)$. WCGNA was applied to 37 ROIs. The parameter values were set as follows: minimum fraction of non-missing samples for a gene to be considered good=0.5 (default), minimum number of non-missing samples for a gene to be considered good=4 (default), minimum number of good genes=4 (default), cut height for removing outlying samples=80 (no samples removed), minimum number of objects on branch to be considered a cluster=2 (cutreeStatic), network type=signed-hybrid, soft power=5, adjacency correlation function=bicor, maxPOutliers=0.05 adjacency distance function=dist (network adjacency default), TOM type=signed, minimum module size (number of genes)=30, dissimilarity threshold used for merging modules: 0.25. The analysis identified 8 distinct modules labelled with colours, plus a module of 2780 unassigned genes (grey module). The WGCNA analysis was performed using R packages: WGCNA V.1.72-1, tidyverse V.2.0.0 and openxlsx V.4.2.5.2.

This analysis identified 8 modules of co-expressed genes ranging from 157 to 2280 genes per module. These modules were characterised by enrichment in GO.BP terms using R package clusterProfiler V.4.8.2, by correlation with cell type abundance determined through cell deconvolution against phenotypes identified by human liver single-cell RNA sequencing analysis and by correlation with estimates of CD45 and HBsAg immunofluorescent staining during GeoMx protocols (online supplemental table 5).

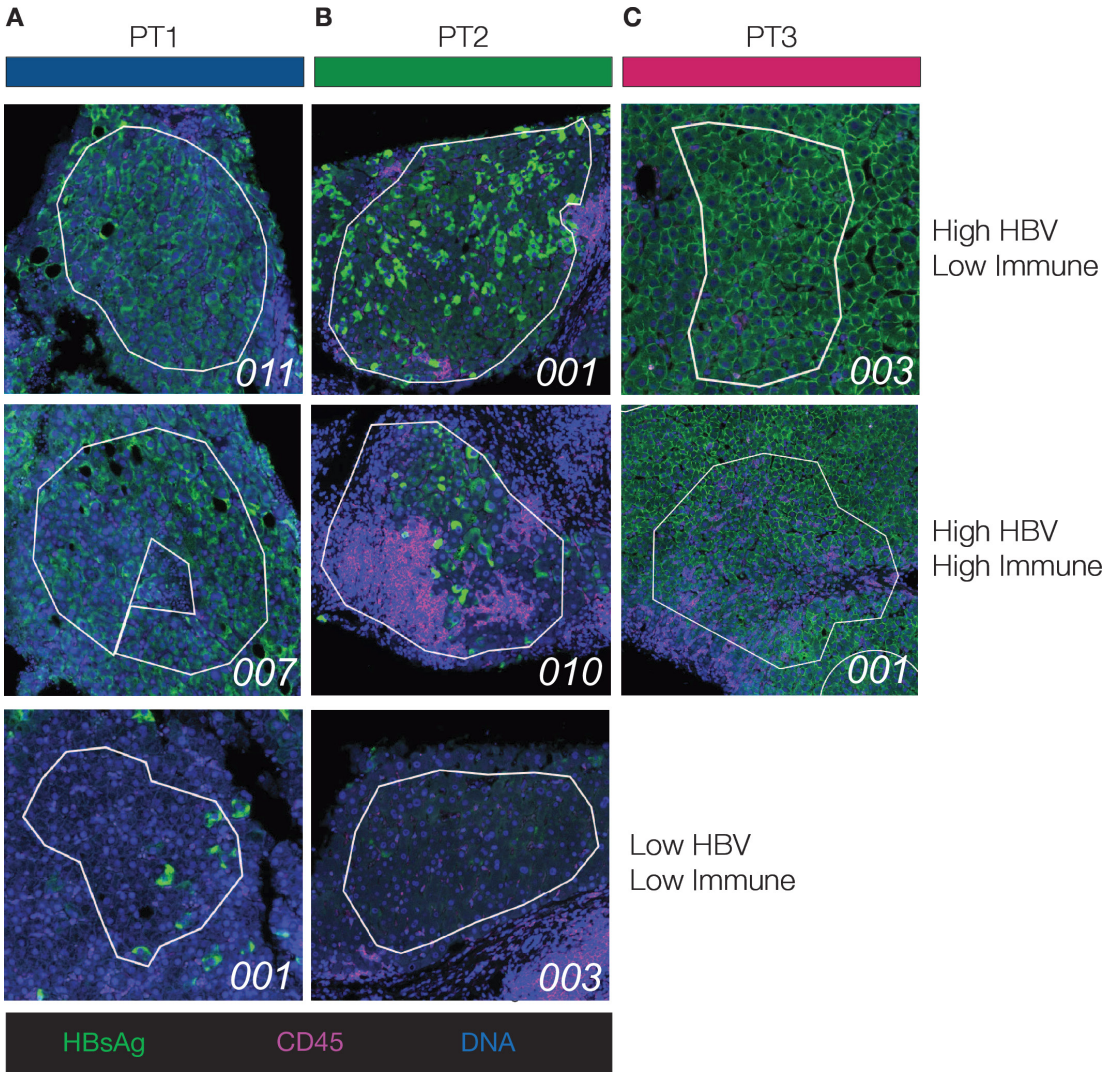

Figure 1 Regions of interest (ROIs) and their classification. Multiplex immunofluorescent images of representative ROIs from each patient are shown (A–C). Regions were classified as either 'low' or 'high' for hepatitis B virus (HBV) or immune infiltrate, based on the abundance of HBV surface antigen (HBsAg)+ and CD45+ cells, respectively. This categorisation was used for all downstream analysis. In the bottom left of each image, the ROI identifier is labelled. In patient (PT)3, there was extensive HBsAg staining with no HBsAg low regions identified.

RESULTS

Study participants have discrete spatial signatures associated with viral and immune features

We studied FFPE liver tissue from three CHB treatment-naïve patients: HBV mono-infection (PT1); HDV/HBV co-infection (PT2) and HIV/HBV co-infection (PT3) (table 1). PT1 in the HBeAg– chronic hepatitis phase had fluctuating ALT levels (20–53 IU/mL) and HBV DNA (6850–190 000 IU/mL) over 2 years. Liver biopsy showed normal architecture with minimal inflammation. Mild steatosis was also present. PT2 with untreated HBV/HDV co-infection for 18 years, and HBeAg+ chronic hepatitis, had moderate levels of HBV DNA and HDV RNA and evidence of advanced fibrosis suggestive of cirrhotic transformation and moderate inflammation. PT3 with HIV/HBV co-infection diagnosed 1 year prior, and HBeAg+ chronic hepatitis had fluctuating ALT levels (151–348 IU/mL) and evidence of marked inflammation with retained liver architecture. Immunofluorescent staining for HBsAg, PTRPC (CD45) and DNA (nuclear stain) guided selection of ROIs for transcriptional profiling, revealing distinct/heterogeneous HBsAg patterns (figure 1A–C and online supplemental figure 1A–C) as previously described.[22 24] PT1 displayed a ground glass appearance of staining, with areas of marginal/submembranous HBsAg staining (figure 1A). PT2 exhibited a clustered distribution of cytoplasmic HBsAg expression, resembling clonally expanded populations[25] (figure 1B). PT3 had a diffuse membranous pattern of HBsAg expression involving the majority of hepatocytes indicative of high replicative HBV status (HBV DNA 235×10^6 IU/mL) (figure 1C).

We assessed immune infiltration and HBsAg expression in selected ROIs in each patient biopsy (figure 1A–C, online supplemental table 1). ROIs averaging 96 871 µm^2 (±44 284 µm^2 SD) with an estimated mean of 412 nuclei

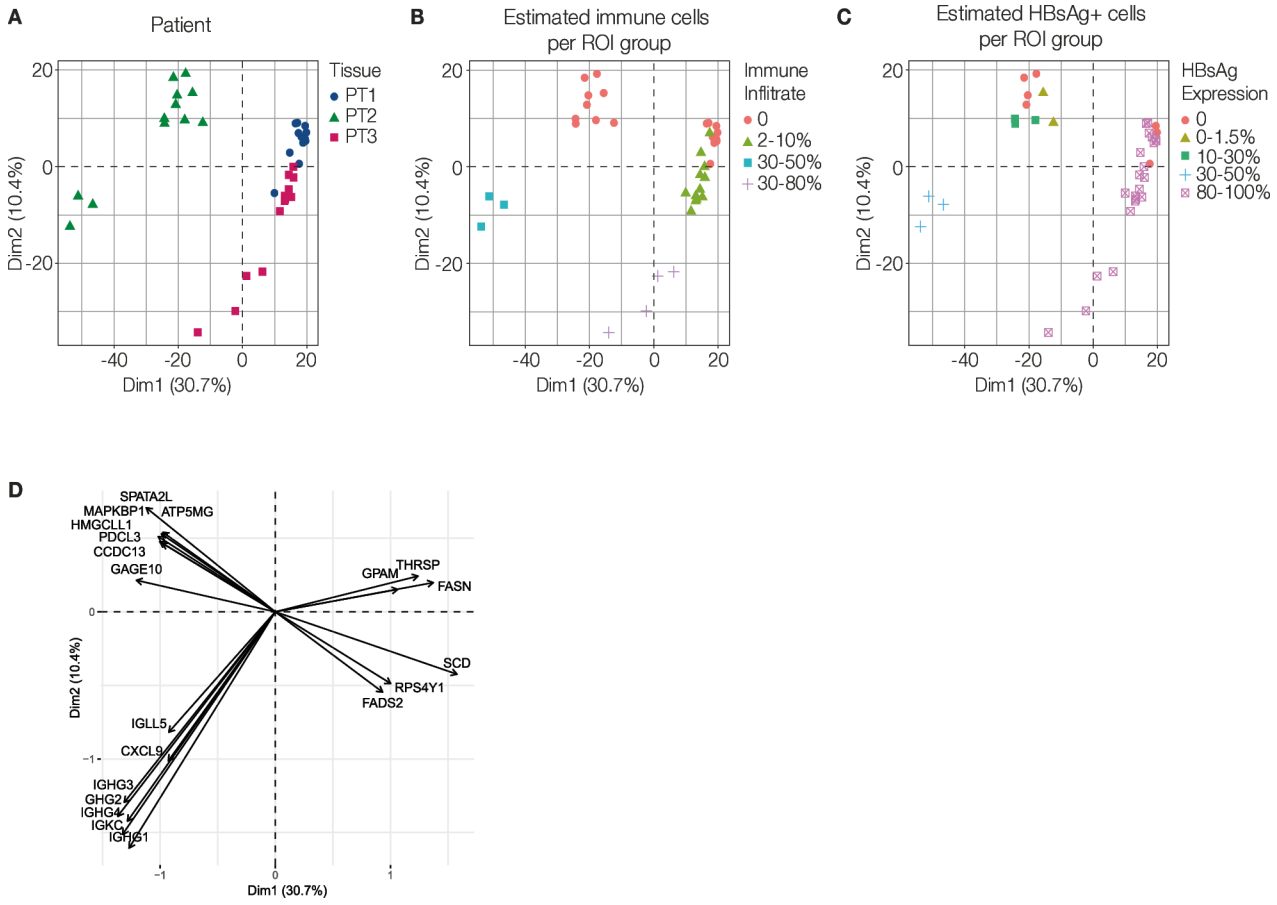

Figure 2 Leucocyte content represents a significant source of variability in the sampled regions of hepatitis B virus (HBV)+ biopsies. The first and second dimensions, produced by principal component analysis of gene expression of the 37 regions of interest (ROIs), are annotated by biopsy (A), estimated frequency of CD45+ cells per ROI group (B) and estimated frequency of HBV surface antigen (HBsAg)+ cells per ROI group (C). Top contributing genes (D).

(±238 nuclei SD; online supplemental figure 2A) demonstrated excellent sequencing quality (online supplemental figure 2B, C) and minimal variation across the whole genome atlas/housekeeping transcripts (online supplemental figure 2D, E). 37 ROIs were categorised according to immune cell (CD45+) and HBsAg+ cell composition and gene expression enriched in each ROI was quantified by the GeoMx Human Whole Transcriptome Atlas assay. PCA indicated variability attributed to donor-specific factors (figure 2A), with 10.4% of the variance associated with immune cell proportions, while 30.7% was associated with HBsAg expression, Ishak score and/or unknown sample-specific differences (figure 2B,C). The first dimension was influenced by genes involved in fatty acid biosynthesis (*SCD, FASN, THRSP, GPAM*). The second dimension was associated with immunoglobulin genes (*IGHG1/2/3/4, IGKC*), human leucocyte antigen genes (*HLA-A/B, HLA-DRA/DQA1/DQB1/DPA1*) and T cell transcripts (*TRBC1, CD8A*) (figure 2D). The third and fourth dimensions only explained 5.4% and 4.4% of the global variance, respectively, and suggested ROI heterogeneity related to hepatocyte zonation (online supplemental figure 3A–C). The third dimension distinguished sample-specific phenotypes between PT1 and PT3 (online supplemental figure 3B). This observation did not associate with the quantity of immune cells or HBsAg+ cells. Instead, the top contributing genes included Kupffer/macrophage-associated transcripts (*C1QC, C1QB, CD5L, HLA-DQA1*) and the zonally expressed hepatocyte genes (*CYP2A6, G0S2 and FASN*) (online supplemental figure 3C). The fourth dimension differentiated a single ROI on the upregulation of canonical hepatocyte zone 3 markers (such as *GLUL* and *CYP3A4*), compared with the relative reduction in hepatocyte zone 1 transcripts such as *SDS, A2M, LEPR, GLS2, TAT* and *HAL* (online supplemental figure 3C).

Differential gene expression identifies immune active profiles within patients

To profile the pathways in spatially heterogenous HBsAg expressing ROIs, in the presence or absence of co-infection, we performed differential expression analysis (figure 3A,B and online supplemental table 3). No differentially expressed genes (DEGs) were observed when comparing HBsAg+ areas with HBsAg− areas, suggesting that subtle viral-induced changes in the liver are not captured with the current number of samples. We therefore assessed DEGs without adjustment for multiple comparisons to identify potential gene candidates impacted by HBV infection. In PT1 (HBeAg−),

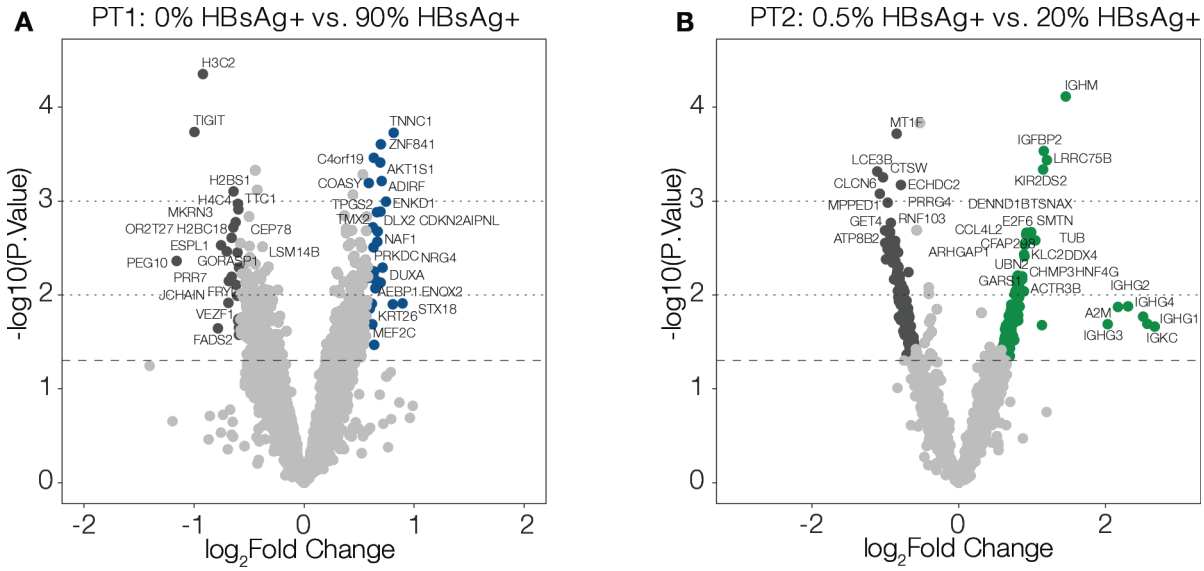

Figure 3 Minimal transcriptional differences between high and low areas of HBV surface antigen (HBsAg) expression. The visual estimates of HBsAg+ cell positivity for each group of regions of interest are indicated above the differential gene expression of each patient biopsy: patient (PT)1 (A) and PT2 (B). Patient-relative areas of low and high HBsAg protein expression were compared. Unadjusted p values are shown; no p values were under 0.05 after adjustment for multiple comparisons. From top to bottom, the horizontal dashed lines show p=0.001, 0.01 and 0.05. HBV, hepatitis B virus.

high HBsAg+/CD45− staining areas showed an upregulation of *ENKD1*, *AKT1S1* and *ADIRF*, involved in microtubule organisation, regulation of cell growth/survival in response to nutrient/hormonal signals and adipogenesis, respectively (figure 3A). *PRDKC*, a DNA damage sensor and effective activator of HBV cccDNA transcription,[26] was also upregulated in these areas (figure 3A). The HBsAg+ areas in PT2 with HDV/HBV co-infection, were associated with immune genes *IGHG1, IGHG2, IGHG3, IGHG4* participating in the 'B cell receptor signalling pathway'. There were very few CD45+ cells visible by immunofluorescence, suggesting an underestimate of immune cell infiltration (figure 3B). No overlapping or conserved upregulated genes were found between PT1 and PT2. PT3 (HIV/HBV co-infection) displayed extensive membranous HBsAg staining with no HBsAg low regions for intratissue comparisons.

Exploring gene enrichment associated with immune cell infiltrate, in PT1 the CD45+ regions showed an upregulation of genes associated with the constant region of immunoglobulin heavy chains (*IGHG1, IGHG2, IGHG3, IGHG4*); a common feature in the immune-rich areas of all samples tested (figure 4A). PT2 was characterised by additional enrichment of genes linked to viral infection and apoptotic process regulation (*USP17L3, USP17L15, USP17L17, CASP1*), along with cellular processing/major histocompatibility complex (MHC) class II presentation (*CD74, HLA-DRB1*) and chemokine genes (*CXCL9, CCL19*) involved in inflammatory responses/homing (figure 4B). In PT3 (HIV/HBV co-infection), immune-enriched areas exhibited increased expression of MHC class II genes (*HLA-DRB1, HLA-DQB1*), including classical and non-classical MHC class I genes (*HLA-B, HLA-A, HLA-E, HLA-F*) (figure 4C). Similar to PT2, the immune-high areas in PT3 showed increased expression of *CXCL9* and *CCL5*, a major HIV suppressive factor, in addition to genes involved in CD8 T cell signalling (*TRBC1, TRAC*), T cell and natural killer (NK) cell cytotoxicity (*NKG7*) and interferon (IFN) transcriptional regulation and response (*IRF1, GBP1*). Notably, 'cell cytotoxicity' and 'B cell receptor signalling pathway' were common across all three patient tissues despite quantifiable differences in leucocyte presence (figure 4D–F and online supplemental table 4), indicating both shared and unique profiles.

Distinct distribution of cellular phenotypes in the profiled ROIs

To assess the composition of the host's immune response, we performed an unbiased analysis of cellular phenotypes present in the profiled ROIs, deconvoluting gene expression patterns based on a training matrix of single-cell sequencing data from the human liver cell atlas (figure 5A–C). Estimated proportions of different cell types showed contribution from hepatocytes and non-parenchymal cells with distinct immune cell distributions localising in high immune areas/HBsAg+ areas. PT1 (HBeAg−) showed lower adaptive and innate immune cell proportions consistent with an inactive disease phase (figure 5A). Differences in immune cell composition were more striking for PT2 with HDV/HBV co-infection (HBeAg+; high fibrosis) showing higher abundance of γδT cells, αβT cells, mature B cells, NK-like and inflammatory macrophages in addition to higher proportions of cholangiocytes and stellate cells relative to the low immune/low HBsAg+ areas (figure 5B). The immune-rich HBsAg+ areas in PT3 (HIV/HBV co-infection) were distinguished by higher abundance of αβT

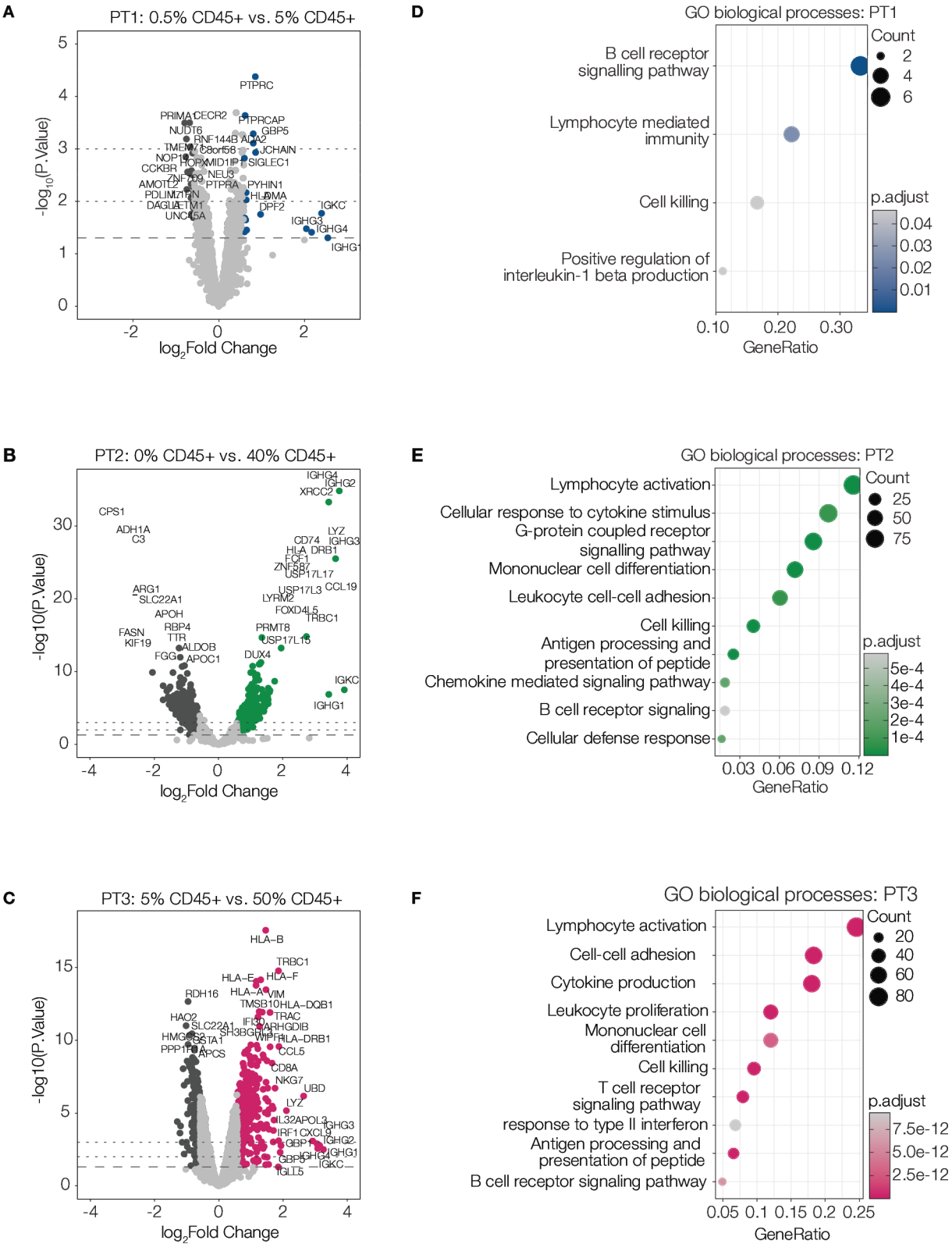

Figure 4 Enrichment of T and B lymphocyte-associated transcripts in areas of inflammation. Areas of low and high immune cell presence were compared in each biopsy. The visual estimates of CD45+ cell positivity for each group of regions of interest are indicated above the differential gene expression of each patient biopsy: patient (PT)1 (A), PT2 (B), PT3 (C). Unadjusted p values are shown; adjusted p values are included in the online supplemental table 4. From top to bottom, the horizontal dashed lines show p=0.001, 0.01 and 0.05. Biological processes associated with the relative high immune cell presence are shown for PT1 (D), PT2 (E) and PT3 (F).

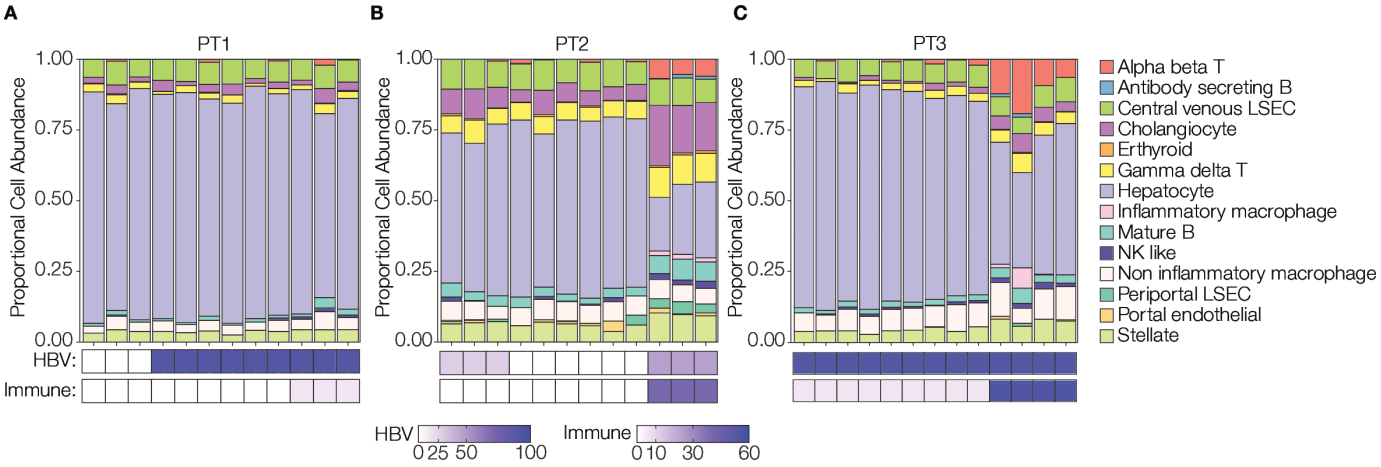

Figure 5 Composition of immune infiltrates in selected regions of tissue biopsies. Proportional cell abundance of adult liver cell populations is estimated for regions of interest (ROIs) in the biopsies from patient (PT)1 (A), PT2 (B) and PT3 (C).

cells and inflammatory macrophages relative to PT2 (HDV/HBV co-infection), as well as the low immune areas within the same donor (figure 5C). Interestingly, the presence of antibody secreting cells was identified in PT2 and PT3 within the immune-rich/high HBsAg areas, although with low abundance.

For unbiased assessment of diverse transcriptomic patterns across the tissues, we used a WGCNA that identified 8 modules of co-expressed genes (range 157–2280 genes per module). Modules were characterised by (i) enrichment in GO.BP terms, (ii) correlation with cell type abundance calculated through cell deconvolution and (iii) estimates of CD45+ and HBsAg+ cells from immunofluorescent staining. This analysis allowed us to establish module identity in all modules with the exception of the Black module. Each tissue displayed distinct transcriptional signatures and module-trait relationships (figure 6A,B, online supplemental figure 4A, B). PT1 (HBeAg–) was characterised by tissue-wide expression of the brown module relating to hepatocyte function and metabolism including fatty acid, cholesterol metabolic process, lipid catabolism and aerobic respiration. PT2 (HDV/HBV co-infection, HBeAg+; high fibrosis) showed tissue-wide expression of the turquoise module enriched for ribosomal transcripts. PT3 (HIV/HBV co-infection; HBeAg+) was distinguished by the red module associated with B cell mediated immunity and phagocytosis (figure 6A,B, online supplemental figure 4A, B). Notably, the red module was upregulated in areas with the highest CD45+ cell counts, distinguishing it from comparable areas in PT2, suggesting that B cell immunity and phagocytosis were more active processes in PT3 with HIV/HBV co-infection (figure 6A and online supplemental figure 4A). Transcripts associating with amino acid metabolism were enriched in the green module, shared by the HDV/HBV and HIV/HBV co-infected samples (PT2 and PT3) in HBsAg high areas with low immune infiltration (figure 6B and online supplemental figure 4A, B). The yellow module, which is associated with lymphocyte activation, B cell signalling and cytotoxicity, was also shared by PT2 and PT3. The presence of CD45+ within a given ROI was strongly associated with the yellow module, containing genes implicated in adhesion, cytokine production, αβ T cell activation, lymphocyte proliferation, cytotoxicity and responses to tumour necrosis factors and type II IFNs reflecting the presence of plasma cells, B cells, αβ and γδT cells, inflammatory macrophages and NK-like cells (figure 6B and online supplemental figure 4A, B).

An increased hepatocyte abundance was associated with the pink, blue and brown modules (online supplemental figure 4B). The pink module that involved genes related to responses to metal, such as zinc or copper, was associated with PT1. The blue module, containing genes characteristic of hepatocyte metabolic and catabolic processes involving fatty acids, alcohol, carboxylic acids, cholesterol and amino acid catabolism, was associated with HBsAg expression and was over-represented in the HBV mono-infected and HIV/HBV samples (PT1 and PT3); however, the correlation is skewed by the high expression and lack of HBsAg heterogeneity within these samples, respectively. Interestingly, PT1 (HBeAg–, low fibrosis tissue) was associated with both the brown and blue modules, displaying comparable metabolic and catabolic pathways, whereas a negative module-trait relationship was observed with PT2 (HDV/HBV co-infection, HBeAg+; high fibrosis), suggesting transcriptional disparities in hepatocytes between samples (online supplemental figure 4A, B).

DISCUSSION

In this proof-of-principle study, we employed spatial transcriptomics, a rapidly emerging technology, to evaluate liver gene signatures relative to specific cell types and associated biological functions in the setting of CHB and co-infection with HDV or HIV. Our results highlight the utility of this approach in interrogating the cellular and molecular pathways that may be involved in disease pathogenesis, and identifying shared and distinctive features.

We used HBsAg staining to identify infected hepatocytes, as it is highly expressed in all phases of infection

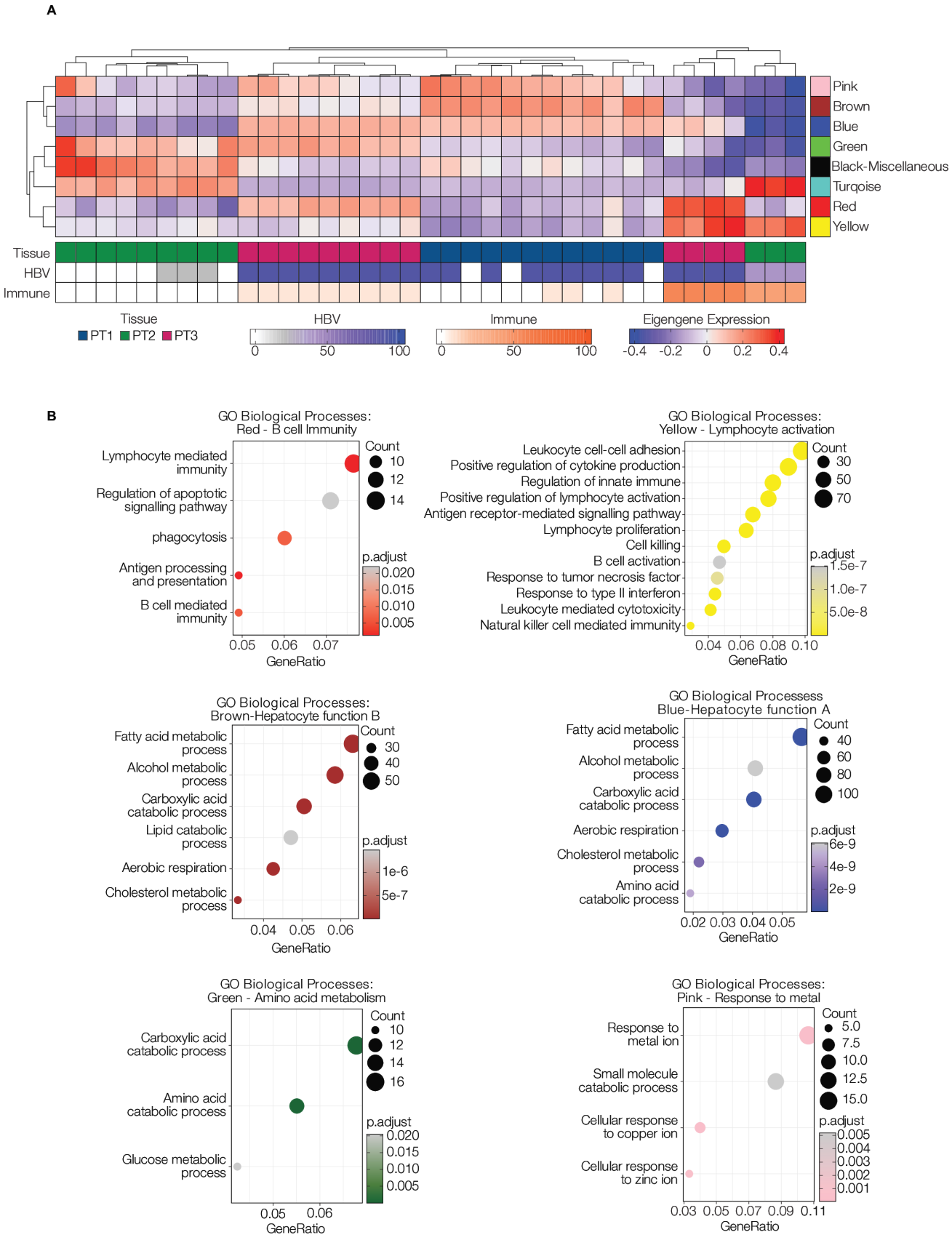

Figure 6 Distinct transcriptional profiles in chronic hepatitis B (CHB) biopsies. Eigengene expression of each module (n=8) produced from a weighted gene correlation network analysis. Eigengene expression is annotated by the estimated HBV surface antigen (HBsAg)+ and CD45+ cell frequency per region of interest (ROI) group and tissue origin (A). The colour-labelled modules of co-expressed genes were evaluated for over-representation of biological processes, of which 6/8 modules were enriched in known GO pathways (B). HBV, hepatitis B virus.

and considered a sensitive biomarker of infection.[27] Our data showed spatially discrete transcriptomic signatures associated with immune features within the liver biopsies. Differential expression analysis highlighted shared features, identifying overlapping genes involved in 'B cell receptor signalling' and 'cytotoxicity'. In the setting of HDV/HBV co-infection (PT2: HBeAg+; high fibrosis), there was an upregulation of genes involved in apoptotic processes and chemokine genes (*CXCL9, CCL19*) involved in the recruitment of activated T cells and B cells. Limited data exist regarding the involvement of B cells in HDV/HBV co-infection. A recent study reported expression of the NK cell receptor NKG2D on HDV-specific and intrahepatic CD8+ T cells that associated with TCR-independent activation.[28] NKG2D expression on CD8+ T cells correlated with liver inflammation, suggesting a non-antigen-specific bystander T cell-related liver inflammation in active HDV/HBV co-infection.[28] This non-specific immune activation and recruitment of activated immune cells in the liver may be a driver for piecemeal necrosis, portal inflammation with the presence of apoptotic bodies.[29]

An upregulation of chemokines genes and MHC class I and II presentation was observed in HIV/HBV co-infection (PT3). Upregulation of *CCL5* as well as genes involved in the transcriptional regulation of the IFN response was specific to HIV/HBV co-infection. Previous studies on Peg-IFNα-treated patients identified intrahepatic IFN signalling and increased CXCL10 and CXCL9 serum levels in individuals who achieved a cure.[30] Interestingly, patients with HIV/HBV co-infection achieve higher rates of HBsAg clearance (up to 12%) relative to HBV mono-infected (<1%), following ART initiation, which may relate to immune reconstitution and intrahepatic immune differences.[31] The distinctive signature observed in the HIV/HBV co-infected sample could potentially be influenced by HIV infection. HIV DNA has been detected in hepatocytes of co-infected patients,[32] suggesting that HIV replication in the liver could potentially contribute to increased HBsAg production and sustained inflammation.

Importantly, deconvoluting the immune cell composition in patient tissues yielded a high-resolution cellular map providing new insights into underinvestigated immune subsets. Immune-high samples showed increased numbers of γδT cells, αβT cells, mature B cells and inflammatory macrophages. The relevant proportions differed between samples, with PT1 with HBeAg–disease, displaying the lowest overall abundance. These observations align with recent work showing variation in intrahepatic immune gene expression during episodes of hepatitis compared with healthy livers.[21] The transcriptomic signature of immune-rich samples with increased proportions of T and B cells and macrophages resembles patterns observed in patients with 'immune tolerant' disease and tertiary lymphoid structures in tumours.[33] B cell infiltration in the liver, constituting approximately 15% of the inflammatory infiltration, can influence T cell-mediated immune tolerance and antibody-associated liver damage contributing to liver inflammation and fibrosis.[34 35] Although the role of γδT cells is less well defined in HBV infection, their increased proportions in HDV/HBV co-infection warrants further investigation to define their role in disease progression/fibrosis and to dissect their beneficial versus pathogenic role.

In addition to accentuated immune gene profiles, our findings identified specific modules upregulated in HDV/HBV co-infection relating to ribosomal activity. HBsAg can upregulate endoplasmic reticulum (ER) stress signalling pathways,[36] induced by prolonged and overwhelming protein production/misfolding, triggering the unfolded protein response, the ER overload response and steroid uptake pathways.[37] This activation could sensitise hepatocytes to cell death and premalignant changes, suggesting that it could be related to hepatocellular carcinogenesis, which is more common in HDV/HBV co-infection.[38]

Transcriptional differences in hepatocytes between samples relating to metabolic function, suggest that perturbations in HBV activity/HBsAg expression could impact several metabolic pathways, leading to a reprogramming of hepatocytes and subsequent clinical disease. Altered metabolic/lipid pathways have been reported in HBV infection,[39] increasing the occurrence of complications, such as HCC and liver steatosis.[40–42]

Our study is limited by the sample size and our findings need to be extended in larger cohorts capturing a wider range of disease phases. Given the heterogeneity of clinical characteristics, the presented findings need to be interpreted with caution and validated in future studies to enable more comprehensive interpatient comparisons and determine their biological significance. Additional research comparing gene expression profiles between fibrotic and non-fibrotic areas could elucidate spatially regulated genes and pathways associated with fibrosis progression in HBV-infected liver tissue. Furthermore, larger cohorts, including non-viral hepatitis control groups, could provide valuable insights into changes attributed to HBV infection. Although we noted differential HBsAg expression in the patients studied, we did not examine HBcAg expression that may identify hepatocytes with active cccDNA transcription.[25] A recent study using spatial transcriptomics by Yu *et al* investigated HBV integrants and demonstrated a reduced frequency of transcriptionally active integrants in patients undergoing antiviral therapy.[43] It would be interesting to see if this is evident in HBV co-infection with HDV and HIV. Future studies using DSP to interrogate the spatial association between HBcAg+ and HBsAg+ cells, and refinement of this approach to identify viral transcripts, may inform us of the niche that renders a cell permissive to infection, and establishment of cccDNA. We were unable to undertake hepatitis D antigen immunostaining, however this would be key in further studies of HBV and in co-infected states with HDV.

Overall, our data demonstrate that spatial transcriptomics is a powerful tool for investigating the molecular

mechanisms of HBV infection in liver tissue. Future research can leverage this analysis to guide HBV treatment modalities, especially in the setting of HDV and HIV co-infection.

Author affiliations
[1]Nuffield Department of Surgical Sciences, University of Oxford, Oxford, UK
[2]Nuffield Department of Medicine, University of Oxford, Oxford, UK
[3]Institute of Immunity and Transplantation, Division of Infection and Immunity, University College London, London, UK
[4]Cancer Research UK, Scotalnd Institute, Glasgow, UK
[5]Division of Infection and Immunity, Barts Health NHS Trust, London, UK
[6]Centre for Immunobiology, Barts & The London School of Medicine & Dentistry, QMUL, London, UK
[7]UCL Cancer Institute, Royal Free London NHS Foundation Trust, London, UK
[8]Chinese Academy of Medical Sciences Oxford Institute, University of Oxford, Oxford, UK

X Dimitra Peppa @peppa_group

Acknowledgements We would like to thank Aaron McClelland and Yan Liang at NanoString for their assistance with the GeoMx workflow.

Contributors AC performed data analysis; AC, JMH, EA-B, CN and AH presented data and drafted the manuscript; RD, FI, AQ, PTFK and JAMcK contributed to data interpretation and critical editing of the manuscript. USG and DP contributed to the conception and design of the study, data interpretation, critical revision of the manuscript and study supervision.

Funding This work was supported by the US Department of Health and Human Services, National Institute of Health/National Institute of Allergy and Infectious Diseases/award (R01AI55182) to DP; an Academy of Medical Sciences Starter Grant (SGL021/1030), Seedcorn funding Rosetrees/Stoneygate Trust (A2903) and Mid-Career Research Award from The Medical Research Foundation (MRF-044-0004-F-GILL-C0823) to USG and Medical Sciences Division (0011187) Pump-Priming grant awarded to FI and JAMcK. Research in the McKeating laboratory is funded by a Wellcome Investigator Award 200838/Z/16/Z, Wellcome Discovery Award 225198/Z/22/Z, Chinese Academy of Medical Sciences Innovation Fund for Medical Science, China (grant number: 2018-I2M-2-002).

Competing interests None declared.

Patient and public involvement Patients and/or the public were not involved in the design, or conduct, or reporting, or dissemination plans of this research.

Patient consent for publication Not applicable.

Ethics approval This study was approved by the local Research Ethics Committee (REC) London Bridge (17/LO/0266). The study complied with all relevant ethical regulations for work with human participants and conformed to the Helsinki Declaration principles and Good Clinical Practice (GCP) guidelines. Participants gave informed consent to participate in the study before taking part.

Provenance and peer review Not commissioned; externally peer reviewed.

Data availability statement Data are available in a public, open access repository. All data relevant to the study are included in the article or uploaded as supplementary information. The NanoString GeoMx DSP raw sequencing data, metadata are deposited at Gene Expression Omnibus series (GSE265785). Annotated scripts for the computational analysis are available at: https://github.com/amyrcross/SpatialHBV/

ORCID iDs
James M Harris http://orcid.org/0000-0003-1880-3496
Dimitra Peppa http://orcid.org/0000-0002-9281-5471

REFERENCES

1 Jeng WJ, Papatheodoridis GV, Lok ASF. Hepatitis B. *Lancet* 2023;401:1039–52.
2 Stockdale AJ, Kreuels B, Henrion MYR, *et al*. The global prevalence of hepatitis D virus infection: systematic review and meta-analysis. *J Hepatol* 2020;73:523–32.
3 Singh KP, Crane M, Audsley J, *et al*. HIV-hepatitis B virus coinfection: epidemiology, pathogenesis, and treatment. *AIDS* 2017;31:2035–52.
4 Thio CL, Seaberg EC, Skolasky R Jr, *et al*. HIV-1, hepatitis B virus, and risk of liver-related mortality in the multicenter cohort study (MACS). *Lancet* 2002;360:1921–6.
5 Colin JF, Cazals-Hatem D, Loriot MA, *et al*. Influence of human immunodeficiency virus infection on chronic hepatitis B in homosexual men. *Hepatology* 1999;29:1306–10.
6 Salmon-Ceron D, Lewden C, Morlat P, *et al*. Liver disease as a major cause of death among HIV infected patients: role of hepatitis C and B viruses and alcohol. *J Hepatol* 2005;42:799–805.
7 Lythgoe KA, Lumley SF, Pellis L, *et al*. Estimating hepatitis B virus cccDNA persistence in chronic infection. *Virus Evol* 2021;7:veaa063.
8 Urban S, Neumann-Haefelin C, Lampertico P. Hepatitis D virus in 2021: virology, immunology and new treatment approaches for a difficult-to-treat disease. *Gut* 2021;70:1782–94.
9 Lim SG, Baumert TF, Boni C, *et al*. The scientific basis of combination therapy for chronic hepatitis B functional cure. *Nat Rev Gastroenterol Hepatol* 2023;20:238–53.
10 Iannacone M, Guidotti LG. Immunobiology and pathogenesis of hepatitis B virus infection. *Nat Rev Immunol* 2022;22:19–32.
11 Vachon A, Osiowy C. Novel biomarkers of hepatitis B virus and their use in chronic hepatitis B patient management. *Viruses* 2021;13:951.
12 van Campenhout MJH, van Bömmel F, Pfefferkorn M, *et al*. Host and viral factors associated with serum hepatitis B virus RNA levels among patients in need for treatment. *Hepatology* 2018;68:839–47.
13 Son MS, Yoo JH, Kwon C-I, *et al*. Associations of expressions of HBcAg and HBsAg with the histologic activity of liver disease and viral replication. *Gut Liver* 2008;2:166–73.
14 Maini MK, Peppa D. Shared immunotherapeutic approaches in HIV and hepatitis B virus: combine and conquer. *Curr Opin HIV AIDS* 2020;15:157–64.
15 Likhitsup A, Lok AS. Understanding the natural history of hepatitis B virus infection and the new definitions of cure and the endpoints of clinical trials. *Clin Liver Dis* 2019;23:401–16.
16 Peppa D, Gill US, Reynolds G, *et al*. Up-regulation of a death receptor renders antiviral T cells susceptible to NK cell-mediated deletion. *J Exp Med* 2013;210:99–114.
17 Genshaft AS, Subudhi S, Keo A, *et al*. Single-cell RNA sequencing of liver fine-needle aspirates captures immune diversity in the blood and liver in chronic hepatitis B patients. *Hepatology* 2023;78:1525–41.
18 Kim SC, Wallin JJ, Ghosheh Y, *et al*. Efficacy of antiviral therapy and host-virus interactions visualised using serial liver sampling with fine-needle aspirates. *JHEP Rep* 2023;5:100817.
19 Testoni B, Roca Suarez AA, Battisti A, *et al*. Evaluation of the HBV liver reservoir with fine needle aspirates. *JHEP Rep* 2023;5:100841.
20 Traum D, Wang YJ, Schwarz KB, *et al*. Highly multiplexed 2-dimensional imaging mass cytometry analysis of HBV-infected liver. *JCI Insight* 2021;6:e146883.
21 van Buuren N, Ramirez R, Turner S, *et al*. Characterization of the liver immune microenvironment in liver biopsies from patients with chronic HBV infection. *JHEP Rep* 2022;4:100388.
22 Aggarwal A, Odorizzi PM, Brodbeck J, *et al*. Intrahepatic quantification of HBV antigens in chronic hepatitis B reveals heterogeneity and treatment-mediated reductions in HBV core-positive cells. *JHEP Rep* 2023;5:100664.
23 Danaher P, Kim Y, Nelson B, *et al*. Advances in mixed cell deconvolution enable quantification of cell types in spatial transcriptomic data. *Nat Commun* 2022;13:385.
24 Hsu HC, Lai MY, Su IJ, *et al*. Correlation of hepatocyte HBsAg expression with virus replication and liver pathology. *Hepatology* 1988;8:749–54.
25 Mason WS, Gill US, Litwin S, *et al*. HBV DNA integration and clonal hepatocyte expansion in chronic hepatitis B patients considered immune tolerant. *Gastroenterology* 2016;151:986–98.

26 Fan Y, Liang Y, Liu Y, *et al*. PRKDC promotes hepatitis B virus transcription through enhancing the binding of RNA Pol II to cccDNA. *Cell Death Dis* 2022;13:404.
27 Hadziyannis E, Laras A. Viral biomarkers in chronic HBeAg negative HBV infection. *Genes (Basel)* 2018;9:469.
28 Kefalakes H, Horgan XJ, Jung MK, *et al*. Liver-resident bystander CD8(+) T cells contribute to liver disease pathogenesis in chronic hepatitis D virus infection. *Gastroenterology* 2021;161:1567–83.
29 Gill US. The immune landscape in hepatitis Delta virus infection-still an open field. *J Viral Hepat* 2023;30 Suppl 1:21–5.
30 Kakimi K, Lane TE, Wieland S, *et al*. Blocking chemokine responsive to gamma-2/interferon (IFN)-gamma inducible protein and monokine induced by IFN-gamma activity in vivo reduces the pathogenetic but not the antiviral potential of hepatitis B virus-specific cytotoxic T lymphocytes. *J Exp Med* 2001;194:1755–66.
31 Chang CC, Crane M, Zhou J, *et al*. HIV and co-infections. *Immunol Rev* 2013;254:114–42.
32 Zerbato JM, Avihingsanon A, Singh KP, *et al*. HIV DNA persists in hepatocytes in people with HIV-hepatitis B co-infection on antiretroviral therapy. *EBioMedicine* 2023;87:104391.
33 Sautès-Fridman C, Petitprez F, Calderaro J, *et al*. Tertiary lymphoid structures in the era of cancer immunotherapy. *Nat Rev Cancer* 2019;19:307–25.
34 Mohamadkhani A, Naderi E, Sotoudeh M, *et al*. Clinical feature of intrahepatic B-lymphocytes in chronic hepatitis B. *Int J Inflam* 2014;2014:896864.
35 Walewska-Zielecka B, Madalinski K, Jablonska J, *et al*. Composition of inflammatory infiltrate and its correlation with HBV/HCV antigen expression. *World J Gastroenterol* 2008;14:4040–6.
36 Lazar C, Uta M, Branza-Nichita N. Modulation of the unfolded protein response by the human hepatitis B virus. *Front Microbiol* 2014;5:433.
37 Bravo R, Parra V, Gatica D, *et al*. Endoplasmic reticulum and the unfolded protein response: dynamics and metabolic integration. *Int Rev Cell Mol Biol* 2013;301:215–90.
38 Li Y, Xia Y, Cheng X, *et al*. Hepatitis B surface antigen activates unfolded protein response in forming ground glass hepatocytes of chronic hepatitis B. *Viruses* 2019;11:386.
39 Svicher V, Salpini R, Piermatteo L, *et al*. Whole exome HBV DNA integration is independent of the intrahepatic HBV reservoir in HBeAg-negative chronic hepatitis B. *Gut* 2021;70:2337–48.
40 Cheng Y-M, Hsieh T-H, Wang C-C, *et al*. Impact of HBV infection on clinical outcomes in patients with metabolic dysfunction-associated fatty liver disease. *JHEP Rep* 2023;5:100836.
41 Hyrina A, Burdette D, Song Z, *et al*. Targeting lipid biosynthesis pathways for hepatitis B virus cure. *PLoS One* 2022;17:e0270273.
42 Schmidt NM, Wing PAC, Diniz MO, *et al*. Targeting human Acyl-CoA:cholesterol acyltransferase as a dual viral and T cell metabolic checkpoint. *Nat Commun* 2021;12:2814.
43 Yu X, Gong Q, Yu D, *et al*. Spatial transcriptomics reveals a low extent of transcriptionally active hepatitis B virus integration in patients with HBsAg loss. *Gut* 2024;73:797–809.